

---

# Data-efficient Hindsight Off-policy Option Learning

---

Markus Wulfmeier<sup>1</sup> Dushyant Rao<sup>1</sup> Roland Hafner<sup>1</sup> Thomas Lampe<sup>1</sup> Abbas Abdolmaleki<sup>1</sup> Tim Hertweck<sup>1</sup>  
Michael Neunert<sup>1</sup> Dhruva Tirumala<sup>1</sup> Noah Siegel<sup>1</sup> Nicolas Heess<sup>1</sup> Martin Riedmiller<sup>1</sup>

## Abstract

We introduce Hindsight Off-policy Options (HO2), a data-efficient option learning algorithm. Given any trajectory, HO2 infers likely option choices and backpropagates through the dynamic programming inference procedure to robustly train all policy components off-policy and end-to-end. The approach outperforms existing option learning methods on common benchmarks. To better understand the option framework and disentangle benefits from both temporal and action abstraction, we evaluate ablations with flat policies and mixture policies with comparable optimization. The results highlight the importance of both types of abstraction as well as off-policy training and trust-region constraints, particularly in challenging, simulated 3D robot manipulation tasks from raw pixel inputs. Finally, we intuitively adapt the inference step to investigate the effect of increased temporal abstraction on training with pre-trained options and from scratch.

## 1. Introduction

Deep reinforcement learning has seen numerous successes in recent years (Silver et al., 2017; OpenAI et al., 2018; Vinyals et al., 2019), but still faces challenges in domains where data is limited or expensive. One candidate solution to address the challenges and improve data efficiency is to impose hierarchical policy structures. By dividing an agent into a combination of low-level and high-level controllers, the options framework (Sutton et al., 1999; Precup, 2000) introduces a form of action abstraction, effectively reducing the high-level controller’s task to choosing from a discrete set of reusable sub-policies. The framework further enables temporal abstraction by explicitly modelling the temporal continuation of low-level behaviors. Unfortunately, in prac-

tice, hierarchical control schemes often introduce technical challenges, including a tendency to learn degenerate solutions preventing the agent from using its full capacity (Harb et al., 2018), undesirable trade-offs between learning efficiency and final performance (Harutyunyan et al., 2019), or the increased variance of updates (Precup, 2000). Additional challenges in off-policy learning for hierarchical approaches (Precup et al., 2006) led to a focus of recent works on the on-policy setting, forgoing the considerable improvements in data efficiency often connected to off-policy methods.

We propose an approach to address these drawbacks, Hindsight Off-policy Options (HO2): a method for data-efficient, robust, off-policy option learning. The algorithm simultaneously learns a high-level controller and low-level options via a single end-to-end optimization procedure. It improves data efficiency by leveraging off-policy learning and inferring distributions over option for trajectories in hindsight to maximize the likelihood of good actions and options.

To facilitate off-policy learning the algorithm does not condition on executed options but treats these as latent variables during optimization and marginalizes over all options to compute the exact likelihood. HO2 backpropagates through the resulting dynamic programming inference graph (conceptually related to (Rabiner, 1989; Shiarlis et al., 2018; Smith et al., 2018)) to enable the training of all policy components from trajectories, independent of the executed option. As an additional benefit, the formulation of the inference graph allows to impose intuitive, hard constraints on the option termination frequency, thereby regularizing the learned solution (and encouraging temporally-extended behaviors) independently of the scale of the reward.

The policy update follows an expectation-maximization perspective and generates an intermediate, non-parametric policy, which is adapted to maximize agent performance. This enables the update of the parametric policy to rely on simple weighted maximum likelihood, without requiring further approximations such as Monte Carlo estimation or continuous relaxation (Li et al., 2019). Finally, the updates are stabilized using adaptive trust-region constraints, demonstrating the importance of robust policy optimization for hierarchical reinforcement learning (HRL) in line with recent work on on-policy option learning (Zhang & Whiteson, 2019).

<sup>1</sup>DeepMind, London, United Kingdom. Correspondence to: Markus Wulfmeier <mwulfmeier@google.com>.

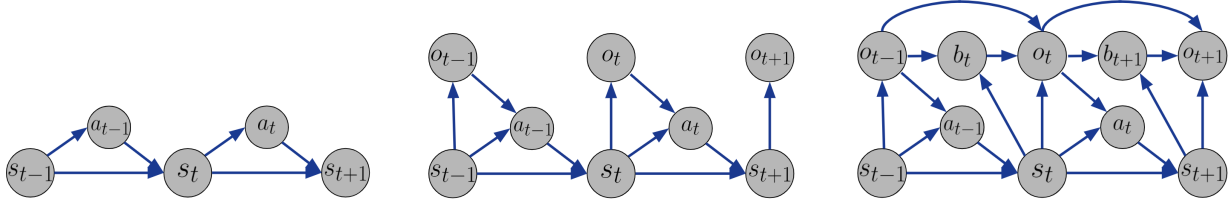


Figure 1: Graphical model for flat policies (left), mixture policies (middle) - introducing a type of action abstraction, and option policies (right) - adding temporal abstraction via autoregressive options. While the action  $a$  is solely dependent on the state  $s$  for flat policies, mixture policies introduce the additional component or option  $o$  which affects the actions (following Equation 1). Option policies do not change the direct dependencies for actions but instead affect the options themselves, which are now also dependent on the previous option and its potential termination  $b$  (following Equation 2).

We experimentally compare HO2 to prior option learning methods. By treating options as latent variables in off-policy learning and enabling backpropagation through the inference procedure, HO2 demonstrates to be more efficient than prior approaches such as the Option-Critic (Bacon et al., 2017) or DAC (Zhang & Whiteson, 2019). HO2 additionally outperforms IOPG (Smith et al., 2018), which considers a similar perspective but still builds on on-policy training. To better understand different abstractions in option learning, we compare with corresponding policy optimization methods for flat policies (Abdolmaleki et al., 2018a) and mixture policies without temporal abstraction (Wulfmeier et al., 2020) thereby allowing us to isolate the benefits of both action and temporal abstraction. Both properties demonstrate particular relevance in more demanding simulated robot manipulation tasks from raw pixel inputs. We further perform extensive ablations to evaluate the impact of trust-region constraints, off-policyness, option decomposition, and the benefits of maximizing temporal abstraction when using pre-trained options versus learning from scratch.

Our main contributions include:

- A robust, efficient off-policy option learning algorithm enabled by a probabilistic inference perspective on HRL. The method outperforms existing option learning methods on common benchmarks and demonstrates benefits on pixel-based 3D robot manipulation tasks.
- An intuitive technique to further encourage temporal abstraction beyond the core method, using the inference graph to constrain option switches without additional weighted loss terms.
- A careful analysis to improve our understanding of the options framework by isolating the impact of action abstraction and temporal abstraction.
- Further ablation and analysis of several algorithmic choices: trust-region constraints, off-policy versus on-policy data, option decomposition, and the importance of temporal abstraction with pre-trained options versus learning from scratch.

## 2. Method

We start by considering a reinforcement learning setting with an agent operating in a Markov Decision Process (MDP) consisting of the state space  $\mathcal{S}$ , the action space  $\mathcal{A}$ , and the transition probability  $p(s_{t+1}|s_t, a_t)$  of reaching state  $s_{t+1}$  from state  $s_t$  when executing action  $a_t$ . The agent’s behavior is commonly described as a conditional distribution with actions  $a_t$  drawn from the agent’s policy  $\pi(a_t|s_t)$ . Jointly, the transition dynamics and policy induce the marginal state visitation distribution  $p(s_t)$ . The discount factor  $\gamma$  together with the reward  $r_t = r(s_t, a_t)$  gives rise to the expected return, which the agent aims to maximize:

$$J(\pi) = \mathbb{E}_{p(s_t), \pi(a_t|s_t)} \left[ \sum_{t=0}^{\infty} \gamma^t r_t \right].$$

### 2.1. Policy Types

Option policies introduce temporal and action abstraction in comparison to commonly-used flat Gaussian policies. Our goal in this work is not only to introduce this additional structure to improve data efficiency but to further understand the impact of the different abstractions. For this purpose, we further study mixture distributions. They represent an intermediate case with only action abstraction, as described in Figure 1.

We begin by covering both policy types in the following paragraphs. First, we focus on computing likelihoods of actions (and options) under a policy. Then, we describe the proposed critic-weighted maximum likelihood algorithm to train hierarchical policies.

**Mixture Policies** This type extends flat policies  $\pi(a_t|s_t)$  by introducing a high-level controller that samples from multiple options (low-level policies) independently at each timestep (Figure 1). The joint probability of actions and options is given as:

$$\pi_{\theta}(a_t, o_t|s_t) = \pi^L(a_t|s_t, o_t) \pi^H(o_t|s_t), \quad (1)$$

where  $\pi^H$  and  $\pi^L$  respectively represent high-level policy (which for the mixture is equal to a Categorical distribution

$\pi^H(o_t|s_t) = \pi^C(o_t|s_t)$  and low-level policy (components of the resulting mixture distribution), and  $o$  is the index of the sub-policy or mixture component.

**Option Policies** This type extends mixture policies by incorporating temporal abstraction. We follow the semi-MDP and *call-and-return* option model (Sutton et al., 1999), defining an option as a triple  $(I(s_t, o_t), \pi^L(a_t|s_t, o_t), \beta(s_t, o_t))$ . The initiation condition  $I$  describes an option’s probability to start in a state and is simplified to  $I(s_t, o_t) = 1 \forall s_t \in \mathcal{S}$  following (Bacon et al., 2017; Zhang & Whiteson, 2019). The termination condition  $b_t \sim \beta(s_t, o_t)$  denotes a Bernoulli distribution describing the option’s probability to terminate in any given state, and the action distribution for a given option is modelled by  $\pi^L(a_t|s_t, o_t)$ . Every time the agent observes a state, the current option’s termination condition is sampled. If subsequently no option is active, a new option is sampled from the controller  $\pi^C(o_t|s_t)$ . Finally, we sample from either the continued or new option to generate a new action. The resulting transition probabilities between options are described by

$$p(o_t|s_t, o_{t-1}) = \begin{cases} 1 - \beta(s_t, o_{t-1})(1 - \pi^C(o_t|s_t)) & \text{if } o_t = o_{t-1} \\ \beta(s_t, o_{t-1})\pi^C(o_t|s_t) & \text{otherwise} \end{cases} \quad (2)$$

During interaction in an environment, an agent samples individual options. However, during learning HO2 takes a probabilistic inference perspective with options as latent variables and states and actions as observed variables. This allows us to infer likely options over a whole trajectory in hindsight, leading to efficient intra-option learning (Precup, 2000) for all options independently of the executed option. This is particularly relevant for off-policy learning, as options can change between data generation and learning.

Following the graphical model in Figure 1 and corresponding transition probabilities in Equation 2, the probability of being in option  $o_t$  at timestep  $t$  across a trajectory  $h_t = \{s_t, a_{t-1}, s_{t-1}, \dots, s_0, a_0\}$  is determined in a recursive manner based on the previous timestep’s option probabilities. For the first timestep, the probabilities are given by the high-level controller  $\pi^H(o_0|h_0) = \pi^C(o_0|s_0)$ . For all consecutive steps are computed as follows for  $M$  options:

$$\tilde{\pi}^H(o_t|h_t) = \sum_{o_{t-1}=1}^M [p(o_t|s_t, o_{t-1}) \pi^H(o_{t-1}|h_{t-1}) \pi^L(a_{t-1}|s_{t-1}, o_{t-1})] \quad (3)$$

The distribution is normalized at each timestep following  $\pi^H(o_t|h_t) = \tilde{\pi}^H(o_t|h_t) / \sum_{o'_t=1}^M \tilde{\pi}^H(o'_t|h_t)$ . Performing this exact marginalization at each timestep is much more efficient than computing independently over all possible sequences of options and reduces variance compared to sampling-based approximations.

Building on the option probabilities, Equation 4 conceptualizes the connection between mixture and option policies.

$$\pi_\theta(a_t, o_t|h_t) = \pi^L(a_t|s_t, o_t) \pi^H(o_t|h_t) \quad (4)$$

In both cases, the low-level policies  $\pi^L$  only depend on the current state. However, where mixtures only depend on the current state  $s_t$  for the high-level probabilities  $\pi^H$ , with options we can take into account compressed information about the history  $h_t$  as facilitated by the previous timestep’s distribution over options  $\pi^H(o_{t-1}|h_{t-1})$ .

This dynamic programming formulation in Equation 3 enables the exact computation of the likelihood of actions and options along off-policy trajectories. We can use automatic differentiation in modern deep learning frameworks (e.g. (Abadi et al., 2016)) to backpropagate through the graph and determine the gradient updates for all policy parameters.

## 2.2. Agent Updates

We continue by describing the policy improvement algorithm, which uses the previously determined option probabilities. The three main steps are: 1) update the critic (Eq. 5); 2) generate an intermediate, non-parametric policy based on the updated critic (Eq. 6); 3) update the parametric policy to align to the non-parametric improvement (Eq. 8). By handling the maximization of expected returns with a closed-loop solution for a non-parametric intermediate policy, the update of the parametric policy can build on simple, weighted maximum likelihood. In essence, we do not rely on differentiating an expectation over a distribution with respect to parameters of the distribution. This enables training a broad range of distributions (including discrete ones) without further approximations such as required when the update relies on the reparametrization trick (Li et al., 2019).

**Policy Evaluation** In comparison to prior work on training mixture policies (Wulfmeier et al., 2020), the critic for option policies is a function of  $s$ ,  $a$ , and  $o$  since the current option influences the likelihood of future actions and thus rewards. Note that even though we express the policy as a function of the history  $h_t$ ,  $Q$  is a function of  $o_t, s_t, a_t$ , since these are sufficient to render the future trajectory independent of the past (see the graphical model in Figure 1). We define the TD(0) objective as

$$\min_{\phi} L(\phi) = \mathbb{E}_{s_t, a_t, o_t \sim \mathcal{D}} [(Q_T - Q_\phi(s_t, a_t, o_t))^2], \quad (5)$$

where the current states, actions, and options are sampled from the current replay buffer  $\mathcal{D}$ . For the 1-step target  $Q_T = r_t + \gamma \mathbb{E}_{s_{t+1}, a_{t+1}, o_{t+1}} [Q'(s_{t+1}, a_{t+1}, o_{t+1})]$ , the expectation over the next state is approximated with the sample  $s_{t+1}$  from the replay buffer, and we estimate

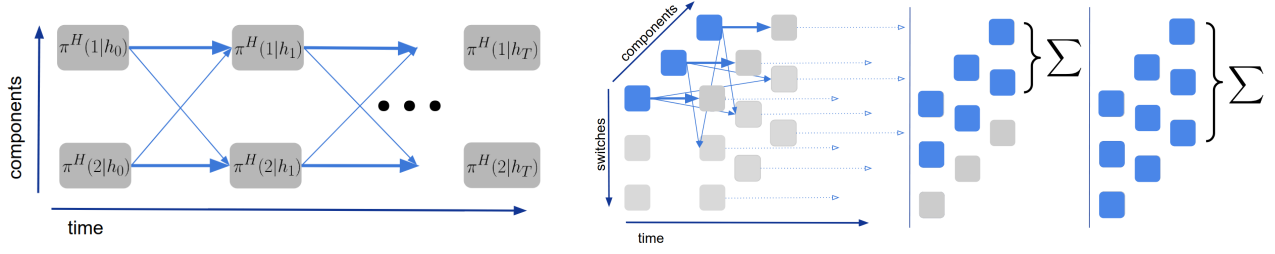


Figure 2: Representation of the dynamic programming forward pass - bold arrows represent connections without switching. Left: example with two options. Right: extension of the graph to explicitly count the number of switches. Marginalization over the dimension of switches determines component probabilities. By limiting over which nodes to sum at every timestep, the optimization can be targeted to fewer switches and more consistent option execution.

the value by sampling actions and options according to  $a_{t+1}, o_{t+1} \sim \pi'(\cdot|h_{t+1})$  following Equation 4.  $\pi'$  and  $Q'$  respectively represent target networks for policy and critic which are used to stabilize training.

**Policy Improvement** We follow an Expectation-Maximization procedure similar to (Wulfmeier et al., 2020; Abdolmaleki et al., 2018b), which first computes an improved non-parametric policy and then updates the parametric policy to match this target. In comparison to prior work, the policy does not only depend on the current state  $s_t$  but also on compressed information about the rest of the previous trajectory  $h_t$ , building on Equation 3. Given the critic, all we require to optimize option policies is the ability to sample from the policy and determine the log-likelihood (gradient) of actions and options under the policy. The first step provides us with a non-parametric policy  $q(a_t, o_t|h_t)$ .

$$\begin{aligned} \max_q J(q) &= \mathbb{E}_{a_t, o_t \sim q, h_t \sim \mathcal{D}} [Q_\phi(s_t, a_t, o_t)], \\ \text{s.t. } \mathbb{E}_{h_t \sim \mathcal{D}} [\text{KL}(q(\cdot|h_t) \parallel \pi_\theta(\cdot|h_t))] &\leq \epsilon_E, \end{aligned} \quad (6)$$

where  $\text{KL}(\cdot \parallel \cdot)$  denotes the Kullback-Leibler divergence, and  $\epsilon_E$  defines a bound on the KL. We can find the solution to the constrained optimization problem in Equation 6 in closed-form and obtain

$$q(a_t, o_t|h_t) \propto \pi_\theta(a_t, o_t|h_t) \exp(Q_\phi(s_t, a_t, o_t)/\eta). \quad (7)$$

Practically speaking, this step computes samples from the previous policy and weights these based on the corresponding temperature-calibrated values of the critic. The temperature parameter  $\eta$  is computed following the dual of the Lagrangian. The derivation and final form of the dual can be found in Appendix C.1, Equation 15.

To align the parametric to the improved non-parametric

policy in the second step, we minimize their KL divergence.

$$\begin{aligned} \theta &= \arg \min_{\theta} \mathbb{E}_{h_t \sim \mathcal{D}} [\text{KL}(q(\cdot|h_t) \parallel \pi_\theta(\cdot|h_t))], \\ \text{s.t. } \mathbb{E}_{h_t \sim \mathcal{D}} [\mathcal{T}(\pi_{\theta+}(\cdot|h_t) \parallel \pi_\theta(\cdot|h_t))] &\leq \epsilon_M \end{aligned} \quad (8)$$

The distance function  $\mathcal{T}$  in Equation 8 has a trust-region effect and stabilizes learning by constraining the change in the parametric policy. The computed option probabilities from Equation 3 are used in Equation 7 to enable sampling of options as well as Equation 8 to determine and maximize the likelihood of samples under the policy. We can apply Lagrangian relaxation again and solve the primal as detailed in Appendix C.2. Finally, we describe the complete pseudocode for HO2 in Algorithm 1.

Note that both Gaussian and mixture policies have been trained in prior work via methods relying on critic-weighted maximum likelihood (Abdolmaleki et al., 2018a; Wulfmeier et al., 2020). By comparing with the extension towards option policies described above, we will make use of this connection to isolate the impact of action abstraction and temporal abstraction in the option framework in Section 3.2.

### 2.3. Maximizing Temporal Abstraction

Persisting with each option over longer time periods can help to reduce the search space and simplify exploration (Sutton et al., 1999; Harb et al., 2018). Previous approaches (e.g. (Harb et al., 2018)) rely on additional weighted loss terms which penalize option transitions.

In addition to the main HO2 algorithm, we introduce an extension mechanism to explicitly limit the maximum number of switches between options along a trajectory to increase temporal abstraction. In comparison to additional loss terms, a parameter for the maximum number of switches can be chosen independently of the reward scale of an environment and provides an intuitive semantic interpretation, both aspects simplify manual adaptation.

We extend the 2D graph for computing option probabilities



**Algorithm 1** Hindsight Off-policy Options

---

**input:** initial parameters for  $\theta$ ,  $\eta$  and  $\phi$ , KL regularization parameters  $\epsilon$ , set of trajectories  $\tau$

**while** not done **do**

    sample trajectories  $\tau$  from replay buffer

    // forward pass along sampled trajectories

    determine component probabilities  $\pi^H(o_t|h_t)$  (Eq. 3)

    sample actions  $a_j$  and options  $o_j$  from  $\pi_\theta(\cdot|h_t)$  (Eq. 4)

    to estimate expectations

    // compute gradients over batch for policy, Lagrangian multipliers and Q-function

$\delta_\theta \leftarrow -\nabla_\theta \sum_{h_t \in \tau} \sum_j [\exp(Q_\phi(s_t, a_j, o_j)/\eta) \log \pi_\theta(a_j, o_j|h_t)]$  following Eq. 7 and 8

$\delta_\eta \leftarrow \nabla_\eta g(\eta) = \nabla_\eta \eta \epsilon + \eta \sum_{h_t \in \tau} \log \sum_j [\exp(Q_\phi(s_t, a_j, o_j)/\eta)]$  following Eq. 15

$\delta_\phi \leftarrow \nabla_\phi \sum_{(s_t, a_t, o_t) \in \tau} (Q_\phi(s_t, a_t, o_t) - Q_T)^2$  following Eq. 5

    update  $\theta, \eta, \phi$  // apply gradient updates

**if** number of iterations = target update **then**

$\pi' = \pi_\theta, Q' = Q_\phi$  // update target networks for policy  $\pi'$  and value function  $Q'$

---

(Figure 2) with a third dimension representing the number of switches between options. Practically, this means that we are modelling  $\pi^H(o_t, n_t|h_t)$  where  $n_t$  represents the number of switches until timestep  $t$ . We can now marginalize over *all* numbers of switches to again determine the option probabilities. Instead, to encourage option consistency across timesteps, we can sum over *only a subset* of nodes for all  $n \leq N$  with  $N$  smaller than the maximal number of switches leading to  $\pi^H(o_t|h_t) = \sum_{n_t=0}^N \pi^H(o_t, n_t|h_t)$ .

For the first timestep, only 0 switches are possible, such that  $\pi^H(o_0, n_0 = 0|h_0) = \pi^C(o_0|s_0)$  and 0 for all other values of  $n$ . For further timesteps, all edges resulting in option terminations  $\beta$  lead to the next step’s option probabilities with increased number of switches  $n_{t+1} = n_t + 1$ . All edges representing the continuation of an option lead to  $n_{t+1} = n_t$ . This results in the computation of the joint

distribution for  $t > 0$ :

$$\tilde{\pi}^H(o_t, n_t|h_t) = \sum_{\substack{o_{t-1}=1, \\ n_{t-1}=1}}^{M,N} p(o_t, n_t|s_t, o_{t-1}, n_{t-1}) \pi^H(o_{t-1}, n_{t-1}|h_{t-1}) \pi^L(a_{t-1}|s_{t-1}, o_{t-1}) \quad (9)$$

which can then be normalized using  $\pi^H(o_t, n_t|h_t) = \tilde{\pi}^H(o_t, n_t|h_t) / \sum_{o'_t=1}^M \sum_{n'_t=1}^L \tilde{\pi}^H(o'_t, n'_t|h_t)$ . The option and switch index transitions  $p(o_t, n_t|s_t, o_{t-1}, n_{t-1})$  are further described in Equation 17 in the Appendix.

### 3. Experiments

In this section, we aim to answer a set of questions to better understand the contribution of different aspects to the performance of option learning - in particular with respect to the proposed method, HO2. To start, in Section 3.1 we explore two questions: (1) How well does HO2 perform in comparison to existing option learning methods? and (2) How important is off-policy training in this context? We use a set of common OpenAI gym (Brockman et al., 2016) benchmarks to answer these questions. In Section 3.2 we ask: (3) How do action abstraction in mixture policies and the additional temporal abstraction brought by option policies individually impact performance? We use more complex, pixel-based 3D robotic manipulation experiments to investigate these two aspects and evaluate scalability with respect to higher dimensional input and state spaces. We also explore: (4) How does increased temporal consistency impact performance, particularly with respect to sequential transfer with pre-trained options? Finally, we perform additional ablations in Section 3.3 to investigate the challenges of robust off-policy option learning and improve understanding of how options decompose behavior based on various environment and algorithmic aspects.

Across domains, we use HO2 to train option policies, RHPO (Wulfmeier et al., 2020) for the reduced case of mixture-of-Gaussians policies with sampling of options at every timestep and MPO (Abdolmaleki et al., 2018a) to train indi-

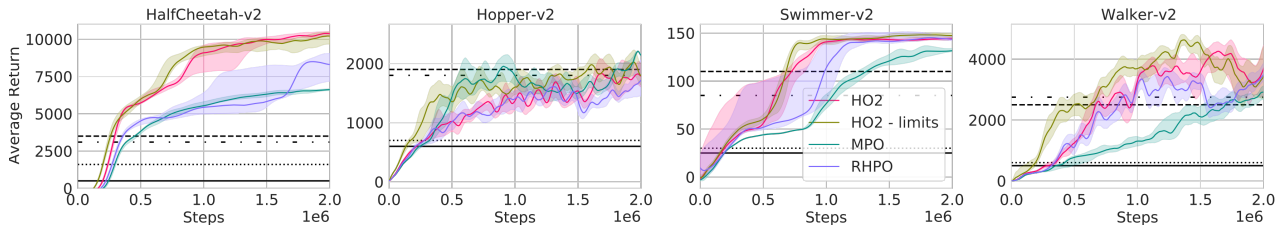


Figure 3: Results on OpenAI gym. Dashed black line represents DAC (Zhang & Whiteson, 2019), dotted line represents Option-Critic (Bacon et al., 2017), solid line represents IOPG (Smith et al., 2018), dash-dotted line represents PPO (Schulman et al., 2017) (approximate results after  $2 \times 10^6$  steps from (Zhang & Whiteson, 2019)). We limit the number of switches to 5 for HO2-limits. HO2 consistently performs better or on par with existing option learning algorithms.

vidual flat Gaussian policies - all based on critic-weighted maximum likelihood estimation for policy optimization.

### 3.1. Comparison of Option Learning Methods

We compare HO2 (with and without limits on option switches) against competitive baselines for option learning in common, feature-based continuous action space domains. HO2 outperforms baselines including Double Actor-Critic (DAC) (Zhang & Whiteson, 2019), Inferred Option Policy Gradient (IOPG) (Smith et al., 2018) and Option-Critic (OC) (Bacon et al., 2017). With PPO (Schulman et al., 2017), we include a commonly used on-policy method for flat policies which in addition serves as the foundation for the DAC algorithm.

As demonstrated in Figure 3, HO2 performs better than or commensurate to existing option learning algorithms such as DAC, IOPG and Option-Critic as well as PPO. Training mixture policies (via RHPO (Wulfmeier et al., 2020)) without temporal abstraction slightly reduces both performance and sample efficiency but still outperforms on-policy methods in many cases. Here, enabling temporal abstraction (even without explicitly maximizing it) provides an inductive bias to reduce the search space for the high-level controller and can lead to more data-efficient learning, such that HO2 even without constraints performs better than RHPO.

Finally, while less data-efficient than HO2, even off-policy learning alone with flat Gaussian policies (here MPO (Abdolmaleki et al., 2018b)) can outperform current on-policy option algorithms, for example in the HalfCheetah and Swimmer domains while otherwise at least performing on par. This emphasizes the importance of a strong underlying policy optimization method.

Using the switch constraints for increasing temporal abstraction from Section 2 can provide minor benefits in some tasks but has overall only a minor effect on performance. We further investigate this setting in sequential transfer in Section 3.2. It has to be noted that given the comparable simplicity of these tasks, considerable performance gains are achieved with pure off-policy training. In the next section, we study more complex domains to isolate additional gains from action and temporal abstraction.

### 3.2. Ablations: Action Abstraction and Temporal Abstraction

We next ablate different aspects of HO2 on more complex simulated 3D robot manipulation tasks - stacking and the more dynamic ball-in-cup (BIC) - as displayed in Figure 4, based on robot proprioception and raw pixel inputs (64x64 pixel, 2 cameras for BIC and 3 for stacking). Since the performance of HO2 for training from scratch is relatively independent of switch constraints (Figure 3), we will sim-

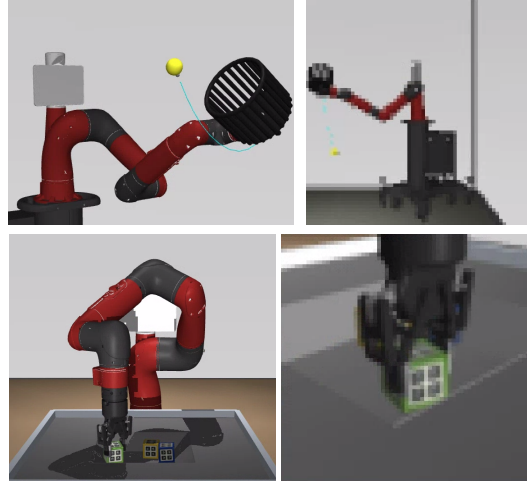


Figure 4: Ball-In-Cup (top) and Stacking (bottom). Left: Environments. Right: Example agent observations.

plify our figures by focusing on the base method. To reduce data requirements, we use a set of common techniques to improve data-efficiency and accelerate learning for all methods. We will apply multi-task learning with a related set of tasks to provide a curriculum, with details in Appendix A. Furthermore, we assign rewards for all tasks to any generated transition data in hindsight to improve data efficiency and exploration (Andrychowicz et al., 2017; Riedmiller et al., 2018; Wulfmeier et al., 2020; Cabi et al., 2017).

Across all tasks, except for simple positioning and reach tasks (see Appendix A), action abstraction improves performance (mixture policies via RHPO versus flat Gaussian policies via MPO). In particular the more challenging stacking tasks shown in Figure 5 intuitively benefit from shared sub-behaviors with easier tasks. Finally, the introduction of temporal abstraction (option policies via HO2 vs mixture policy via RHPO) further improves both performance and sample efficiency, especially on the more complex stacking tasks. The ability to learn explicit termination conditions, which can be understood as classifiers between two conditions, instead of the high-level controller, as classifier between all options, can considerably simplify the learning problem.

**Optimizing for Temporal Abstraction** There is a difference between simplifying the representation of temporal abstraction for the agent and explicitly maximizing it. The ability to represent temporally abstract behavior in HO2 via the use of explicit termination conditions consistently helps in prior experiments. However, these experiments show limited benefit when increasing temporal consistency (by limiting the number of switches following Section 2.3) for training from scratch.

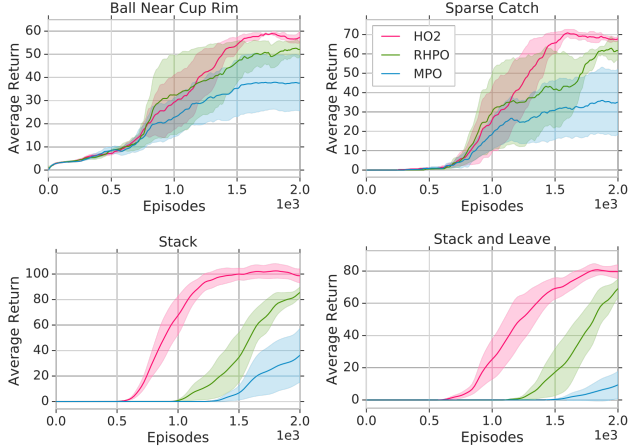


Figure 5: Results for option policies, and ablations via mixture policies, and single Gaussian policies (respectively HO2, RHPO, and MPO) with pixel-based ball-in-cup (left) and pixel-based block stacking (right). All four tasks displayed use sparse binary rewards, such that the obtained reward represents the number of timesteps where the corresponding condition - such as the ball is in the cup - is fulfilled. See Appendix B for details and additional tasks.

In this section, we further evaluate temporal abstraction for sequential transfer with pre-trained options. We first train low-level options for all tasks except for the most complex task in each domain by applying HO2. Next, given a set of pre-trained options, we only train the final task and compare training with and without maximizing temporal abstraction. We use the domains from Section 3.2, block stacking and BIC. As shown in Figure 6, we can see that more consistent options lead to increased performance in the transfer domain. Intuitively, increased temporal consistency and fewer switches lead to a smaller search space from the perspective of the high-level controller.

While the same mechanism should also apply for training from scratch, we hypothesize that the added complexity of simultaneously learning the low-level behaviors (while maximizing temporal consistency) outweighs the benefits. Finding a set of options which not only solve a task but also represent temporally consistent behavior can be harder, and require more data, than just solving the task.

### 3.3. Ablations: Off-policy, Robustness, Decomposition

In this section, we investigate different algorithmic aspects to get a better understanding of the method, properties of the learned options, and how to achieve robust training in the off-policy setting.

**Off-policy Option Learning** In off-policy hierarchical RL, the low-level policy underlying an option can change after trajectories are generated. This results in a non-

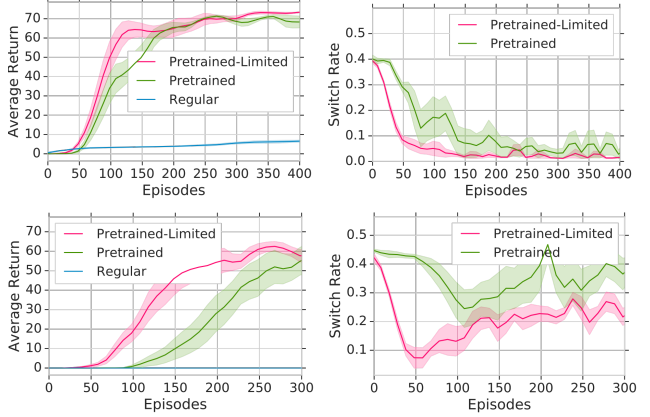


Figure 6: The sequential transfer experiments for temporal abstraction show considerable improvements for limited switches. Top: BIC. Bottom: Stack. In addition, we visualize the actual agent option switch rate in the environment to directly demonstrate the constraint’s effect.

stationarity for training the high-level controller. In addition, including previously executed actions in the forward computation for component probabilities can introduce additional variance into the objective. In practice, we find that removing the conditioning on low-level probabilities (the  $\pi_L$  terms in Equation 3) improves performance and stability. The effect is displayed in Figure 7, where the conditioning of high-level component probabilities on low-level action probabilities (see Section 2) is detrimental.

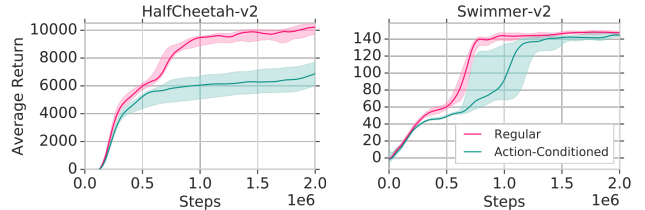


Figure 7: Results on OpenAI gym with/without option probabilities being conditioned on past actions.

We additionally evaluate this effect in the on-policy setting in Appendix A.4 and find its impact to be diminished, demonstrating the connection between the effect and an off-policy setting. While we apply this simple heuristic for HO2, the problem has led to various off-policy corrections for goal-based HRL (Nachum et al., 2018b; Levy et al., 2017) which provide a valuable direction for future work.

**Trust-regions and Robustness** Previous work has shown the benefits of applying trust-region constraints for policy updates of non-hierarchical policies (Schulman et al., 2015; Abdolmaleki et al., 2018b). In this section, we vary the

strength of constraints on the option probability updates (both termination conditions  $\beta$  and the high-level controller  $\pi_C$ ). As displayed in Figure 8, the approach is robust across multiple orders of magnitude, but very weak or strong constraints can considerably degrade performance. Note that a high value is essentially equal to not using a constraint and causes very low performance. Therefore, option learning here relies strongly on trust-region constraints. Further experiments can be found in Appendix A.5.

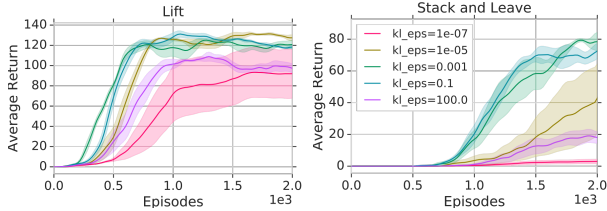


Figure 8: Block stacking results for two tasks with different trust-region constraints. Note that the importance of constraints increases for more complex tasks.

**Decomposition and Option Clustering** To investigate how HO2 uses its capacity and decomposes behavior into options, we apply it to a variety of simple and interpretable locomotion tasks. In these tasks, the agent body (“Ball”, “Ant”, or “Quadruped”) must go to one of three targets in a room, with the task specified by the target locations and a selected target index. As shown for the “Ant” case in Figure 9, we find that option decomposition intuitively depends on both the task properties and algorithm settings. In particular *information asymmetry* (IA), achieved by providing task information only to the high-level controller, can address degenerate solutions and lead to increased diversity with respect to options (as shown by the histogram over options) and more specialized options (represented by the clearer clustering of samples in action space). We can measure this quantitatively, using (1) the Silhouette score, a measure of clustering accuracy based on inter- and intra-cluster distances<sup>1</sup>; and (2) entropy over the option histogram, to quantify diversity. These metrics are reported in Table 1 for all bodies, with and without information asymmetry. The results show that for all cases, IA leads to greater option diversity and clearer separation of option clusters with respect to action space, state space, and task.

More extensive experiments and discussion can be found in Appendix A.1, including additional quantitative and qualitative results for the other bodies and scenarios. To summarize,

<sup>1</sup>The silhouette score is a value in  $[-1, 1]$  with higher values indicating cluster separability. We note that the values obtained in this setting do not correspond to high *absolute* separability, as multiple options can be used to model the same skill or behavior abstraction. We are instead interested in the *relative* clustering score for different scenarios.

the analyses yield a number of relevant observations, showing that (1) for simpler bodies like a “Ball”, the options are interpretable (forward torque, and turning left/right at different rates); and (2) applying the switch constraint introduced in Section 3.2 leads to increased temporal abstraction without reducing the agent’s ability to solve the task.

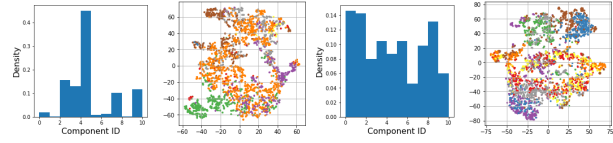


Figure 9: Analysis on Ant locomotion tasks, showing histogram over options, and t-SNE scatter plots in action space colored by option. Left: without IA. Right: with IA. Agents with IA use more components and show clearer option clustering in the action space.

Scenario		Option entropy	s (action)	s (state)	s (task)
Ball	No IA	$1.80 \pm 0.21$	$-0.30 \pm 0.04$	$-0.25 \pm 0.14$	$-0.13 \pm 0.05$
	With IA	$2.23 \pm 0.03$	$-0.13 \pm 0.04$	$-0.11 \pm 0.04$	$-0.05 \pm 0.00$
Ant	No IA	$1.60 \pm 0.08$	$-0.12 \pm 0.02$	$-0.15 \pm 0.07$	$-0.08 \pm 0.03$
	With IA	$2.22 \pm 0.04$	$-0.05 \pm 0.01$	$-0.05 \pm 0.01$	$-0.05 \pm 0.01$
Quad	No IA	$1.55 \pm 0.29$	$-0.07 \pm 0.04$	$-0.12 \pm 0.03$	$-0.11 \pm 0.02$
	With IA	$2.23 \pm 0.04$	$-0.03 \pm 0.03$	$-0.03 \pm 0.00$	$-0.05 \pm 0.01$

Table 1: Quantitative results indicating the diversity of options used (entropy), and clustering accuracy in action and state spaces (silhouette score  $s$ ), with and without information asymmetry (IA). Switching constraints are applied in all cases. Higher values indicate greater separability by option / component.

## 4. Related Work

Hierarchy has been investigated in many forms in reinforcement learning to improve data gathering as well as data fitting aspects. Goal-based approaches commonly define a grounded interface between high- and low-level policies. The high level acts by providing goals to the low level, which is trained to achieve these goals (Dayan & Hinton, 1993; Levy et al., 2017; Nachum et al., 2018a;b; Vezhnevets et al., 2017), effectively generating separate objectives and improving exploration. These methods have been able to overcome very sparse reward domains but commonly require domain knowledge to define the interface. In addition, a hand-crafted interface can limit expressiveness of achievable behaviors.

Non-crafted, emergent interfaces within policies have been investigated from an RL-as-inference perspective via policies with continuous latent variables (Haarnoja et al., 2018; Hausman et al., 2018; Heess et al., 2016; Igl et al., 2019; Tirumala et al., 2019; Teh et al., 2017). Related to these



approaches, we provide a probabilistic inference perspective to off-policy option learning and benefit from efficient dynamic programming inference procedures. We furthermore build on the related idea of information asymmetry (Pinto et al., 2017; Galashov et al., 2018; Tirumala et al., 2019) - providing a part of the observations only to a part of the model. The asymmetry can lead to an information bottleneck affecting the properties of learned low-level policies. We build on the intuition and demonstrate how option diversity can be affected in ablations in Section 3.3.

At its core, our work builds on and investigates the option framework (Precup, 2000; Sutton et al., 1999), which can be seen as describing policies with an autoregressive, discrete latent space. Option policies commonly use a high-level controller to choose from a set of options or skills. These options additionally include termination conditions to enable a skill to represent temporally extended behavior. Without termination conditions, options can be seen as equivalent to components under a mixture distribution, and this simplified formulation has been applied successfully in different methods (Agostini & Celaya, 2010; Daniel et al., 2016; Wulfmeier et al., 2020).

Recent work has also investigated temporally extended low-level behaviours of fixed length (Frans et al., 2018; Li et al., 2019; Nachum et al., 2018b), which do not learn the option duration or termination condition. With HO2, enabling to optimize the extension of low-level behaviour in the option framework provides additional flexibility and removes the engineering effort of choosing the right hyperparameters.

The option framework has been further extended and improved for more practical application (Bacon et al., 2017; Harb et al., 2018; Harutyunyan et al., 2019; Precup et al., 2006; Riemer et al., 2018; Smith et al., 2018). HO2 relies on off-policy training and treats options as latent variables. This enables backpropagation through the option inference procedure and considerable improvements in comparison to efficient than approaches relying on on-policy updates and on-option learning purely for executed options. Related, IOPG (Smith et al., 2018) also considers an inference perspective but only includes on-policy results which naturally have poorer data efficiency. Finally, the benefits of options and other modular policy styles have also been applied in the supervised case for learning from demonstration (Fox et al., 2017; Krishnan et al., 2017; Shiarlis et al., 2018).

One important step to increase the robustness of option learning has been taken in (Zhang & Whiteson, 2019) by building on robust (on-policy) policy optimization with PPO (Schulman et al., 2017). HO2 has similar robustness benefits, but additionally improves data-efficiency by building on off-policy learning, hindsight inference of options, and additional trust-region constraints (Abdolmaleki et al., 2018b; Wulfmeier et al., 2020). Related inference procedures have

also been investigated in imitation learning (Shiarlis et al., 2018) as well as on-policy RL (Smith et al., 2018).

In addition to inferring options in hindsight, off-policy learning enables us to assign rewards for multiple tasks, which has been successfully applied with flat, non-hierarchical policies (Andrychowicz et al., 2017; Riedmiller et al., 2018; Cabi et al., 2017) and goal-based hierarchical approaches (Levy et al., 2017; Nachum et al., 2018b).

## 5. Conclusions

We introduce a robust, efficient algorithm for off-policy training of option policies. The approach outperforms recent work in option learning on common benchmarks and is able to solve complex, simulated robot manipulation tasks from raw pixel inputs more reliably than competitive baselines. HO2 takes a probabilistic inference perspective to option learning, infers option and action probabilities for trajectories in hindsight, and performs critic-weighted maximum-likelihood estimation by backpropagating through the inference step. Being able to infer options for a given trajectory allows robust off-policy training and determination of updates for all instead of only for the executed options. It also makes it possible to impose constraints on the termination frequency independently of an environment’s reward scale.

We separately analyze the impact of action abstraction (via mixture policies), and temporal abstraction (via options). We find that each abstraction independently improves performance. Additional maximization of temporal consistency for option choices is beneficial when transferring pre-trained options but displays a limited effect when learning from scratch. Furthermore, we investigate the consequences of the off-policy nature of training data and demonstrate the benefits of trust-region constraints for option learning. We examine the impact of different agent and environment properties (such as information asymmetry, tasks, and embodiments) with respect to task decomposition and option clustering; a direction which provides opportunities for further investigation in the future. Finally, since our method is based on (weighted) maximum likelihood estimation, it can be adapted naturally to learn structured behavior representations in mixed data regimes, e.g. to learn from combinations of demonstrations, logged data, and online trajectories. This opens up promising directions for future work.

## Acknowledgments

The authors would like to thank Peter Humphreys, Satinder Baveja, Tobias Springenberg, and Yusuf Aytaar for helpful discussion and relevant feedback which helped to shape the publication. We additionally like to acknowledge the support of the DeepMind robotics lab for infrastructure and engineering support.

## References

- Abadi, M., Barham, P., Chen, J., Chen, Z., Davis, A., Dean, J., Devin, M., Ghemawat, S., Irving, G., Isard, M., et al. Tensorflow: A system for large-scale machine learning. In *12th {USENIX} Symposium on Operating Systems Design and Implementation ({OSDI} 16)*, pp. 265–283, 2016.
- Abdolmaleki, A., Springenberg, J. T., Degraeve, J., Bohez, S., Tassa, Y., Belov, D., Heess, N., and Riedmiller, M. Relative entropy regularized policy iteration. *arXiv preprint arXiv:1812.02256*, 2018a.
- Abdolmaleki, A., Springenberg, J. T., Tassa, Y., Munos, R., Heess, N., and Riedmiller, M. A. Maximum a posteriori policy optimisation. *CoRR*, abs/1806.06920, 2018b.
- Agostini, A. and Celaya, E. Reinforcement learning with a gaussian mixture model. In *The 2010 International Joint Conference on Neural Networks (IJCNN)*, pp. 1–8. IEEE, 2010.
- Andrychowicz, M., Wolski, F., Ray, A., Schneider, J., Fong, R., Welinder, P., McGrew, B., Tobin, J., Abbeel, P., and Zaremba, W. Hindsight experience replay. In *Advances in Neural Information Processing Systems*, pp. 5048–5058, 2017.
- Bacon, P.-L., Harb, J., and Precup, D. The option-critic architecture. In *Thirty-First AAAI Conference on Artificial Intelligence*, 2017.
- Brockman, G., Cheung, V., Pettersson, L., Schneider, J., Schulman, J., Tang, J., and Zaremba, W. Openai gym. *ArXiv*, abs/1606.01540, 2016.
- Cabi, S., Colmenarejo, S. G., Hoffman, M. W., Denil, M., Wang, Z., and Freitas, N. The intentional unintentional agent: Learning to solve many continuous control tasks simultaneously. In *Conference on Robot Learning*, pp. 207–216. PMLR, 2017.
- Daniel, C., Neumann, G., Kroemer, O., and Peters, J. Hierarchical relative entropy policy search. *The Journal of Machine Learning Research*, 17(1):3190–3239, 2016.
- Dayan, P. and Hinton, G. E. Feudal reinforcement learning. In *Advances in neural information processing systems*, pp. 271–278, 1993.
- Fox, R., Krishnan, S., Stoica, I., and Goldberg, K. Multi-level discovery of deep options. *arXiv preprint arXiv:1703.08294*, 2017.
- Frans, K., Ho, J., Chen, X., Abbeel, P., and Schulman, J. Meta learning shared hierarchies. In *International Conference on Learning Representations*, 2018.
- Galashov, A., Jayakumar, S. M., Hasenclever, L., Tirumala, D., Schwarz, J., Desjardins, G., Czarnecki, W. M., Teh, Y. W., Pascanu, R., and Heess, N. Information asymmetry in kl-regularized rl. 2018.
- Haarnoja, T., Hartikainen, K., Abbeel, P., and Levine, S. Latent space policies for hierarchical reinforcement learning. In *International Conference on Machine Learning*, pp. 1846–1855, 2018.
- Harb, J., Bacon, P.-L., Klissarov, M., and Precup, D. When waiting is not an option: Learning options with a deliberation cost. In *Thirty-Second AAAI Conference on Artificial Intelligence*, 2018.
- Harutyunyan, A., Dabney, W., Borsa, D., Heess, N., Munos, R., and Precup, D. The termination critic. *CoRR*, abs/1902.09996, 2019. URL <http://arxiv.org/abs/1902.09996>.
- Hausman, K., Springenberg, J. T., Wang, Z., Heess, N., and Riedmiller, M. Learning an embedding space for transferable robot skills. In *International Conference on Learning Representations*, 2018.
- Heess, N., Wayne, G., Tassa, Y., Lillicrap, T., Riedmiller, M., and Silver, D. Learning and transfer of modulated locomotor controllers. *arXiv preprint arXiv:1610.05182*, 2016.
- Igl, M., Gambardella, A., Nardelli, N., Siddharth, N., Böhm, W., and Whiteson, S. Multitask soft option learning. *arXiv preprint arXiv:1904.01033*, 2019.
- Krishnan, S., Fox, R., Stoica, I., and Goldberg, K. Ddco: Discovery of deep continuous options for robot learning from demonstrations. *arXiv preprint arXiv:1710.05421*, 2017.
- Levy, A., Konidaris, G., Platt, R., and Saenko, K. Learning multi-level hierarchies with hindsight. *arXiv preprint arXiv:1712.00948*, 2017.
- Li, A. C., Florensa, C., Clavera, I., and Abbeel, P. Sub-policy adaptation for hierarchical reinforcement learning. *arXiv preprint arXiv:1906.05862*, 2019.
- Nachum, O., Gu, S., Lee, H., and Levine, S. Near-optimal representation learning for hierarchical reinforcement learning. *arXiv preprint arXiv:1810.01257*, 2018a.
- Nachum, O., Gu, S. S., Lee, H., and Levine, S. Data-efficient hierarchical reinforcement learning. In *Advances in Neural Information Processing Systems*, pp. 3303–3313, 2018b.
- OpenAI, Andrychowicz, M., Baker, B., Chociej, M., Józefowicz, R., McGrew, B., Pachocki, J. W., Pachocki, J.,

- Petron, A., Plappert, M., Powell, G., Ray, A., Schneider, J., Sidor, S., Tobin, J., Welinder, P., Weng, L., and Zaremba, W. Learning dexterous in-hand manipulation. *CoRR*, abs/1808.00177, 2018. URL <http://arxiv.org/abs/1808.00177>.
- Pinto, L., Andrychowicz, M., Welinder, P., Zaremba, W., and Abbeel, P. Asymmetric actor critic for image-based robot learning. *arXiv preprint arXiv:1710.06542*, 2017.
- Precup, D. *Temporal abstraction in reinforcement learning*. University of Massachusetts Amherst, 2000.
- Precup, D., Paduraru, C., Koop, A., Sutton, R. S., and Singh, S. P. Off-policy learning with options and recognizers. In Weiss, Y., Schölkopf, B., and Platt, J. C. (eds.), *Advances in Neural Information Processing Systems 18*, pp. 1097–1104. MIT Press, 2006.
- Rabiner, L. R. A tutorial on hidden markov models and selected applications in speech recognition. *Proceedings of the IEEE*, 77(2):257–286, 1989.
- Riedmiller, M., Hafner, R., Lampe, T., Neunert, M., Degraeve, J., Van de Wiele, T., Mnih, V., Heess, N., and Springenberg, J. T. Learning by playing-solving sparse reward tasks from scratch. *arXiv preprint arXiv:1802.10567*, 2018.
- Riemer, M., Liu, M., and Tesauro, G. Learning abstract options. In *Advances in Neural Information Processing Systems*, pp. 10424–10434, 2018.
- Schulman, J., Levine, S., Moritz, P., Jordan, M., and Abbeel, P. Trust region policy optimization. In *Proceedings of the 32nd International Conference on International Conference on Machine Learning-Volume 37*, pp. 1889–1897. JMLR. org, 2015.
- Schulman, J., Wolski, F., Dhariwal, P., Radford, A., and Klimov, O. Proximal policy optimization algorithms. *arXiv preprint arXiv:1707.06347*, 2017.
- Shiarlis, K., Wulfmeier, M., Salter, S., Whiteson, S., and Posner, I. Taco: Learning task decomposition via temporal alignment for control. In *International Conference on Machine Learning*, pp. 4661–4670, 2018.
- Silver, D., Schrittwieser, J., Simonyan, K., Antonoglou, I., Huang, A., Guez, A., Hubert, T., Baker, L., Lai, M., Bolton, A., et al. Mastering the game of go without human knowledge. *Nature*, 550(7676):354, 2017.
- Smith, M., Hoof, H., and Pineau, J. An inference-based policy gradient method for learning options. In *International Conference on Machine Learning*, pp. 4703–4712, 2018.
- Sutton, R., Precup, D., and Singh, S. Between mdps and semi-mdps: A framework for temporal abstraction in reinforcement learning. *Artificial intelligence*, 112(1-2): 181–211, 1999.
- Teh, Y. W., Bapst, V., Czarnecki, W. M., Quan, J., Kirkpatrick, J., Hadsell, R., Heess, N., and Pascanu, R. Distral: Robust multitask reinforcement learning. *CoRR*, abs/1707.04175, 2017. URL <http://arxiv.org/abs/1707.04175>.
- Tirumala, D., Noh, H., Galashov, A., Hasenclever, L., Ahuja, A., Wayne, G., Pascanu, R., Teh, Y. W., and Heess, N. Exploiting hierarchy for learning and transfer in kl-regularized rl. *arXiv preprint arXiv:1903.07438*, 2019.
- Vezhnevets, A. S., Osindero, S., Schaul, T., Heess, N., Jaderberg, M., Silver, D., and Kavukcuoglu, K. Feudal networks for hierarchical reinforcement learning. In *Proceedings of the 34th International Conference on Machine Learning-Volume 70*, pp. 3540–3549. JMLR. org, 2017.
- Vinyals, O., Babuschkin, I., Czarnecki, W. M., Mathieu, M., Dudzik, A., Chung, J., Choi, D. H., Powell, R., Ewalds, T., Georgiev, P., et al. Grandmaster level in starcraft ii using multi-agent reinforcement learning. *Nature*, 575 (7782):350–354, 2019.
- Wulfmeier, M., Abdolmaleki, A., Hafner, R., Springenberg, J. T., Neunert, M., Siegel, N., Hertweck, T., Lampe, T., Heess, N., and Riedmiller, M. Compositional Transfer in Hierarchical Reinforcement Learning. In *Proceedings of Robotics: Science and Systems*, Corvallis, Oregon, USA, July 2020. doi: 10.15607/RSS.2020.XVI.054.
- Zhang, S. and Whiteson, S. Dac: The double actor-critic architecture for learning options. In *Advances in Neural Information Processing Systems*, pp. 2010–2020, 2019.

## Supplementary Material

### A. Additional Experiments

#### A.1. Decomposition and Option Clustering

We further deploy HO2 on a set of simple locomotion tasks, where the goal is for an agent to move to one of three randomized target locations in a square room. These are specified as a set of target locations and a task index to select the target of interest.

The main research questions we aim to answer (both qualitatively and quantitatively) are: (1) How do the discovered options specialize and represent different behaviors?; and (2) How is this decomposition affected by variations in the task, embodiment, or algorithmic properties of the agent? To answer these questions, we investigate a number of variations:

- Three bodies: a quadruped with two (“Ant”) or three (“Quad”) torque-controlled joints on each leg, and a rolling ball (“Ball”) controlled by applying yaw and forward roll torques.
- With or without *information asymmetry* (IA) between high- and low-level controllers, where the task index and target positions are withheld from the options and only provided to the categorical option controller.
- With or without a limited number of switches in the optimization.

Information-asymmetry (IA) in particular, has recently been shown to be effective for learning general skills (Galashov et al., 2018): by withholding task-information from low-level options, they can learn task-agnostic, temporally-consistent behaviors that can be composed by the option controller to solve a task. This mirrors the setup in the aforementioned Sawyer tasks, where the task information is only fed to the high-level controller.

For each of the different cases, we qualitatively evaluate the trained agent over 100 episodes, and generate histograms over the different options used, and scatter plots to indicate how options cluster the state/action spaces and task information. We also present quantitative measures (over 5 seeds) to accompany these plots, in the form of (1) Silhouette score, a measure of clustering accuracy based on inter- and intra-cluster distances<sup>2</sup>; and (2) entropy over the option histogram, to quantify diversity. The quantitative results are shown in Table 2, and the qualitative plots are shown in Figure 10. Details and images of the environment are in Section B.4.

<sup>2</sup>The silhouette score is a value in  $[-1, 1]$  with higher values

The results show a number of trends. Firstly, the usage of IA leads to a greater diversity of options used, across all bodies. Secondly, with IA, the options tend to lead to specialized actions, as demonstrated by the clearer option separation in action space. In the case of the 2D action space of the ball, the options correspond to turning left or right (y-axis) at different forward torques (x-axis). Thirdly, while the simple Ball can learn these high-level body-agnostic behaviors, the options for more complex bodies have greater switch rates that suggest the learned behaviors may be related to lower-level motor behaviors over a shorter timescale. Lastly, limiting the number of switches during marginalization does indeed lead to a lower switch rate between options, without hampering the ability of the agent to complete the task.

#### A.2. Action and Temporal Abstraction Experiments

The complete results for all pixel and proprioception based multitask experiments for ball-in-cup and stacking can be respectively found in Figures 11 and 12. Both RHPO and HO2 outperform a simple Gaussian policy trained via MPO. HO2 additionally improves performance over mixture policies (RHPO) demonstrating that the ability to learn temporal abstraction proves beneficial in these domains. The difference grows as the task complexity increases and is particularly pronounced for the final stacking tasks.

#### A.3. Task-agnostic Terminations

The perspective of options as task-independent skills with termination conditions as being part of a skill, leads to termination conditions which are also task independent. We show that at least in this limited set of experiments, the perspective of task-dependent termination conditions - i.e. with access to task information - which can be understood as part of the high-level control mechanism for activating options improves performance. Intuitively, by removing task information from the termination conditions, we constrain the space of solutions which first accelerates training slightly but limits final performance. It additionally shows that while we benefit when sharing options across tasks, each task gains from controlling the length of these options independently. Based on these results, the termination conditions across all other multi-task experiments are conditioned on the active task.

The complete results for all experiments with task-agnostic terminations can be found in Figure 13.

indicating cluster separability. We note that the values obtained in this setting do not correspond to high *absolute* separability, as multiple options can be used to model the same skill or behavior abstraction. We are instead interested in the *relative* clustering score for different scenarios.



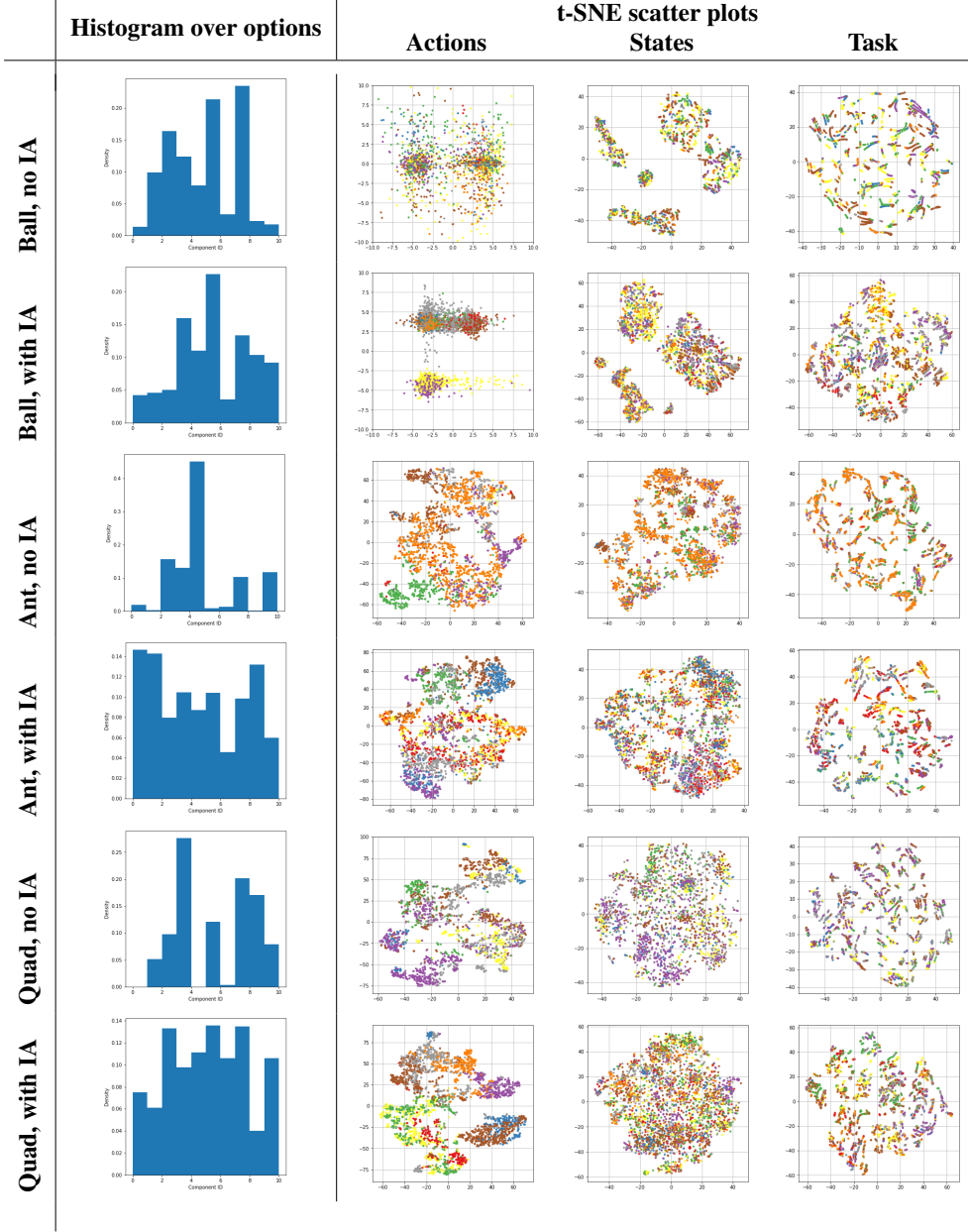


Figure 10: Qualitative results for the three bodies (Ball, Ant, Quad) without limited switches, both with and without IA, obtained over 100 evaluation episodes. **Left:** the histogram over different options used by each agent; **Centre to right:** scatter plots of the action space, state space, and task information, colored by the corresponding option selected. Each of these spaces has been projected to  $2D$  using t-SNE, except for the two-dimensional action space for Ball, which is plotted directly. For each case, care has been taken to choose a median / representative model out of 5 seeds.

#### A.4. Off-Policy Option Learning

In order to train in a more on-policy regime, we reduce the size of the replay buffer by two orders of magnitude and increase the ratio between data generation (actor steps) and data fitting (learner steps) by one order of magnitude. The resulting algorithm is run without any additional hy-

perparameter tuning to provide an insight into the effect of conditioning on action probabilities under options in the inference procedure. We can see that in the on-policy case the impact of this change is less pronounced. Across all cases, we were unable to generate significant performance gains by including action conditioning into the inference procedure.

	Scenario		Option entropy	Switch rate	Cluster score (actions)	Cluster score (states)	Cluster score (tasks)
Regular	Ball	No IA	2.105 ± 0.074	0.196 ± 0.010	−0.269 ± 0.058	−0.110 ± 0.025	−0.056 ± 0.011
		With IA	2.123 ± 0.066	0.346 ± 0.024	−0.056 ± 0.024	−0.164 ± 0.051	−0.057 ± 0.008
	Ant	No IA	1.583 ± 0.277	0.268 ± 0.043	−0.148 ± 0.034	−0.182 ± 0.068	−0.075 ± 0.011
		With IA	2.119 ± 0.073	0.303 ± 0.019	−0.053 ± 0.021	−0.066 ± 0.024	−0.052 ± 0.006
	Quad	No IA	1.792 ± 0.127	0.336 ± 0.019	−0.078 ± 0.064	−0.113 ± 0.035	−0.089 ± 0.050
		With IA	2.210 ± 0.037	0.403 ± 0.014	0.029 ± 0.029	−0.040 ± 0.003	−0.047 ± 0.006
Limited Switches	Ball	No IA	1.804 ± 0.214	0.020 ± 0.009	−0.304 ± 0.040	−0.250 ± 0.135	−0.131 ± 0.049
		With IA	2.233 ± 0.027	0.142 ± 0.015	−0.132 ± 0.035	−0.113 ± 0.043	−0.053 ± 0.003
	Ant	No IA	1.600 ± 0.076	0.073 ± 0.014	−0.124 ± 0.017	−0.155 ± 0.067	−0.084 ± 0.034
		With IA	2.222 ± 0.043	0.141 ± 0.015	−0.052 ± 0.011	−0.054 ± 0.014	−0.050 ± 0.007
	Quad	No IA	1.549 ± 0.293	0.185 ± 0.029	−0.075 ± 0.036	−0.126 ± 0.030	−0.112 ± 0.022
		With IA	2.231 ± 0.042	0.167 ± 0.025	−0.029 ± 0.029	−0.032 ± 0.004	−0.053 ± 0.009

Table 2: Quantitative results indicating the diversity of options used (entropy), and clustering accuracy in action and state spaces (silhouette score), with and without information asymmetry (IA), and with or without limited number of switches. Higher values indicate greater separability by option / component.

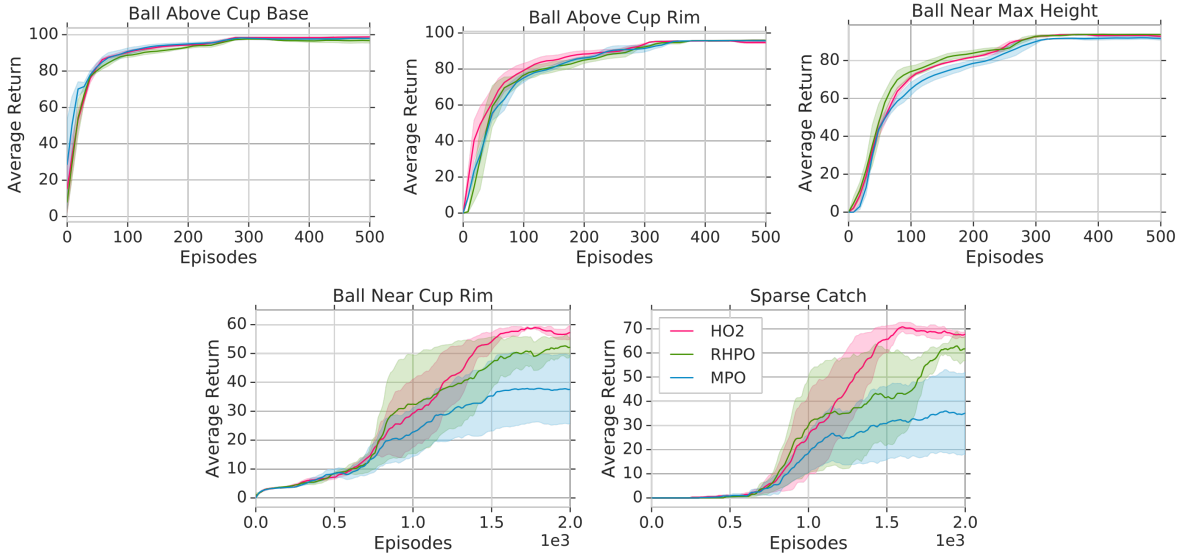


Figure 11: Complete results on pixel-based ball-in-cup experiments.

The complete results for all experiments with and without the action-conditional inference procedure can be found in Figure 14.

### A.5. Trust-region Constraints

The complete results for all trust-region ablation experiments can be found in Figure 15.

With the exception of very high or very low constraints, the approach trains robustly, but performance drops considerably when we remove the constraint fully.

### A.6. Single Time-Step vs Multi Time-Step Inference

To investigate the impact of probabilistic inference of posterior option distributions  $\pi_H(o_t|h_t)$  along the whole sampled

trajectory instead of using sampling-based approximations until the current timestep, we perform additional ablations displayed in Figure 16. Note that we are required to perform probabilistic inference for at least one step to use backpropagation through the inference step to update our policy components. Any completely sampling-based approach would require a different policy optimizer (e.g. via likelihood ratio or reparametrization trick) which would introduce additional compounding effects.

We compare HO2 with an ablated version where we do not compute the option probabilities along the trajectory following Equation 3 but instead use an approximation with only concrete option samples propagating across timesteps for all steps until the current step. To generate action samples, we therefore sample options for every timestep along

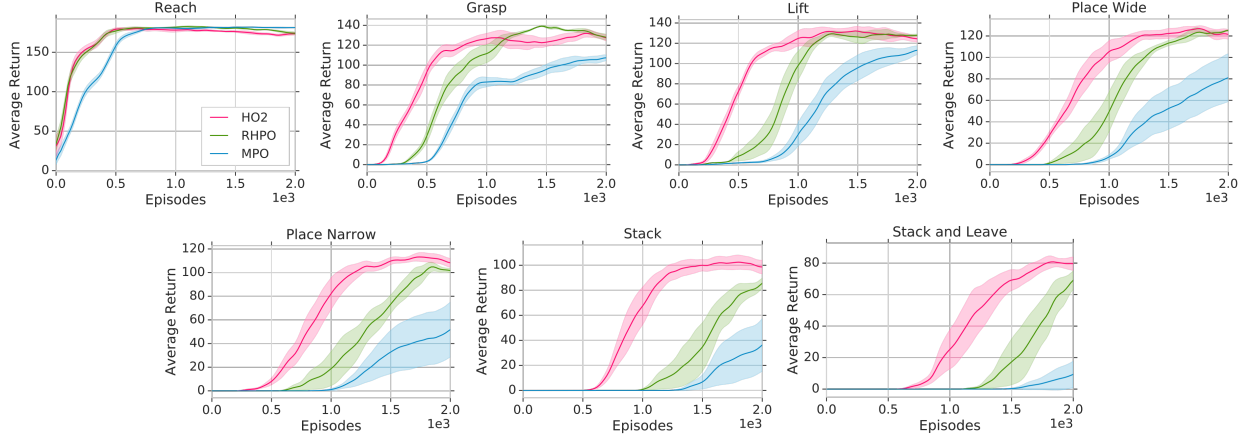


Figure 12: Complete results on pixel-based stacking experiments.

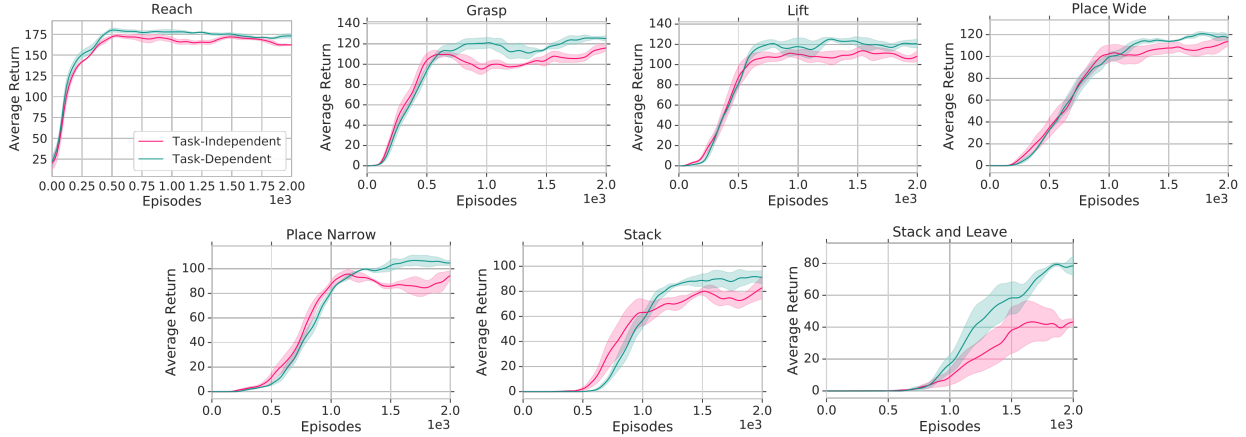


Figure 13: Complete results on multi-task block stacking with and without conditioning termination conditions on tasks.

a trajectory without keeping a complete distribution over options and sample actions only from the active option at every timestep. To determine the likelihood of actions and options for every timestep, we rely on Equation 2 based the sampled options of the previous timestep. By using samples and the critic-weighted update procedure from Equation 8, we can only generate gradients for the policy for the current timestep instead of backpropagating through the whole inference procedure. We find that using both samples from executed options reloaded from the buffer as well as new samples during learning can reduce performance depending on the domain. However, in the Hopper-v2 environment, sampling during learning performs slightly better than inferring options.

## B. Additional Experiment Details

### B.1. OpenAI Gym Experiments

All experiments are run with asynchronous learner and actors. We use a single actor and report performance over the number of transitions generated. Following (Wulfmeier et al., 2020), both HO2 and RHPO use different biases for the initial mean of all options or mixture components - distributed between minimum and maximum action output. This provides a small but non-negligible benefit and supports specialization of individual options. In line with our baselines (DAC (Zhang & Whiteson, 2019), IOPG (Smith et al., 2018), Option Critic (Bacon et al., 2017)) we use 4 options or mixture components for the OpenAI gym experiments. We run all experiments with 5 samples and report variance and mean. All experiments are run with a single actor in a distributed setting. The variant with limited switches limits to 2 switches over a sequence length of 8. Lower and higher values led to comparable results.

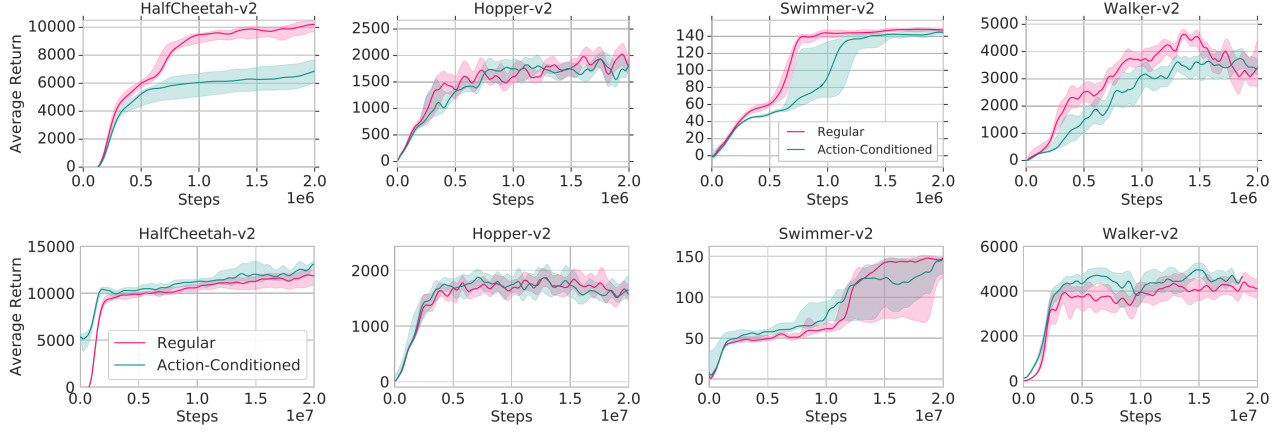


Figure 14: Complete results on OpenAI gym with and without conditioning component probabilities on past executed actions. For the off-policy (top) and on-policy case (bottom). The on-policy approaches uses data considerably less efficiently and the x-axis is correspondingly adapted.

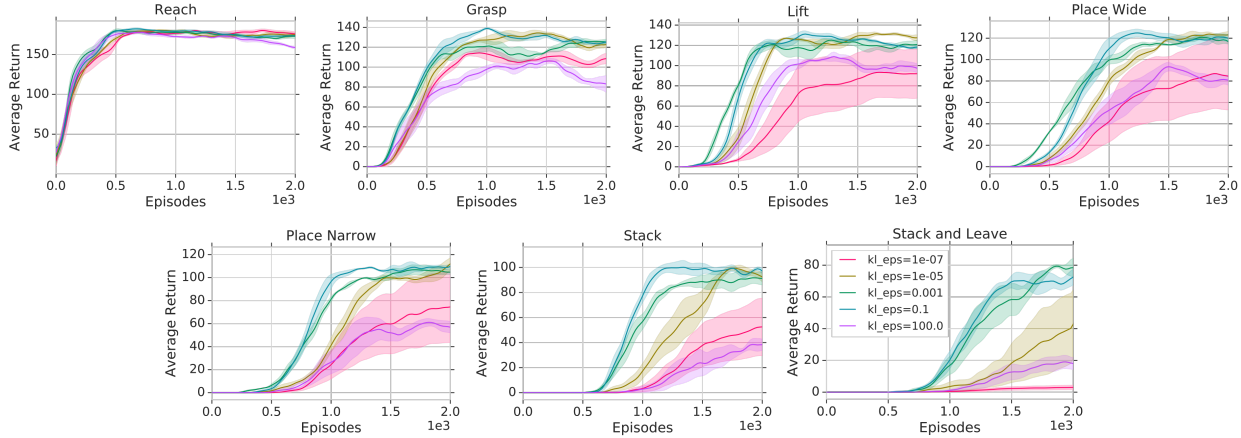


Figure 15: Complete results on block stacking with varying trust-region constraints for both termination conditions  $\beta$  and the high-level controller  $\pi_C$ .

## B.2. Action and Temporal Abstraction Experiments

Shared across all algorithms, we use 3-layer convolutional policy and Q-function torsos with [128, 64, 64] feature channels, [(4, 4), (3, 3), (3, 3)] as kernels and stride 2. For all multitask domains, we build on information asymmetry and only provide task information as input to the high-level controller and termination conditions to create additional incentive for the options to specialize. The Q-function has access to all observations (see the corresponding tables in this section). We follow (Riedmiller et al., 2018; Wulfmeier et al., 2020) and assign rewards for all possible tasks to trajectories when adding data to the replay buffer independent of the generating policy.

**Stacking** The setup consists of a Sawyer robot arm mounted on a table and equipped with a Robotiq 2F-85

parallel gripper. In front of the robot there is a basket of size 20x20 cm which contains three cubes with an edge length of 5 cm (see Figure 4).

The agent is provided with proprioception information for the arm (joint positions, velocities and torques), and the tool center point position computed via forward kinematics. For the gripper, it receives the motor position and velocity, as well as a binary grasp flag. It also receives a wrist sensor’s force and torque readings. Finally, it is provided with three RGB camera images at  $64 \times 64$  resolution. At each timestep, a history of two previous observations (except for the images) is provided to the agent, along with the last two joint control commands. The observation space is detailed in Table 6. All stacking experiments are run with 50 actors in parallel and reported over the current episodes generated by any actor. Episode lengths are up to 600 steps.



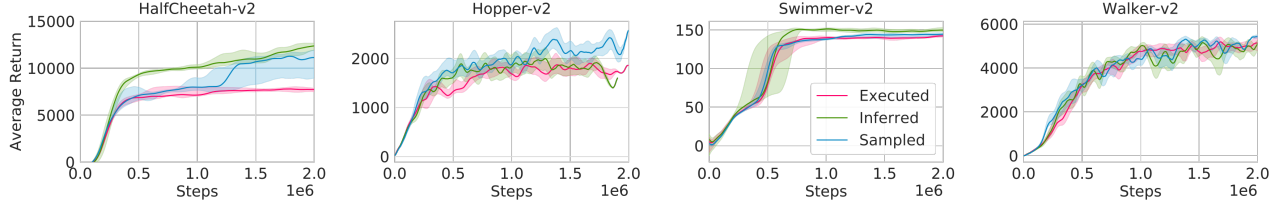


Figure 16: Ablation results comparing inferred options with sampled options during learning (sampled) and during execution (executed). The ablation is run with five actors instead of a single one as used in the OpenAI gym experiments in order to generate results faster.

Hyperparameters	HO2	RHPO	MPO
Policy net		256-256	
Number of actions samples		20	
Q function net		256-256	
Number of components		4	NA
$\epsilon$		0.1	
$\epsilon_\mu$		5e-4	
$\epsilon_\Sigma$		5e-5	
$\epsilon_\alpha$		1e-4	NA
$\epsilon_t$	1e-4	NA	
Discount factor ( $\gamma$ )		0.99	
Adam learning rate		3e-4	
Replay buffer size		2e6	
Target network update period		200	
Batch size		256	
Activation function		elu	
Layer norm on first layer		Yes	
Tanh on output of layer norm		Yes	
Tanh on actions (Q-function)		Yes	
Sequence length		8	

Table 3: Hyperparameters - OpenAI gym

Hyperparameters	HO2	RHPO	MPO
Policy torso			
(shared across tasks)	256		512
Policy task-dependent heads	100 (cat.)		200
Policy shared heads	100 (comp.)		NA
Policy task-dependent terminations	100 (term.)	NA	NA
$\epsilon_\mu$		1e-3	
$\epsilon_\Sigma$		1e-5	
$\epsilon_\alpha$		1e-4	NA
$\epsilon_t$	1e-4	NA	
Number of action samples		20	
Q function torso (shared across tasks)		400	
Q function head (per task)		300	
Number of components		number of tasks	NA
Replay buffer size		1e6	
Target network update period		500	
Batch size		256	

Table 4: Hyperparameters. Values are taken from the OpenAI gym experiments with the above mentioned changes.

Table 5: Action space for the Sawyer Stacking experiments.

$$stol(v, \epsilon, r) = \begin{cases} 1 & \text{iff } |v| < \epsilon \\ 1 - \tanh^2\left(\frac{\tanh(\sqrt{0.95})}{r}|v|\right) & \text{else} \end{cases} \quad (10)$$

$$slin(v, \epsilon_{min}, \epsilon_{max}) = \begin{cases} 0 & \text{iff } v < \epsilon_{min} \\ 1 & \text{iff } v > \epsilon_{max} \\ \frac{v - \epsilon_{min}}{\epsilon_{max} - \epsilon_{min}} & \text{else} \end{cases} \quad (11)$$

$$btol(v, \epsilon) = \begin{cases} 1 & \text{iff } |v| < \epsilon \\ 0 & \text{else} \end{cases} \quad (12)$$

Entry	Dims	Unit	Range
Translational Velocity in x, y, z	3	m/s	[-0.07, 0.07]
Wrist Rotation Velocity	1	rad/s	[-1, 1]
Finger speed	1	tics/s	[-255, 255]

- *REACH(G)*:  $stol(d(TCP, G), 0.02, 0.15)$ :  
Minimize the distance of the TCP to the green cube.
- *GRASP*:  
Activate grasp sensor of gripper ("inward grasp signal" of Robotiq gripper)

Table 6: Observations for the Sawyer Stacking experiments. The TCP’s pose is represented as its world coordinate position and quaternion. In the table,  $m$  denotes meters,  $rad$  denotes radians, and  $q$  refers to a quaternion in arbitrary units ( $au$ ).

Entry	Dims	Unit	History
Joint Position (Arm)	7	rad	2
Joint Velocity (Arm)	7	rad/s	2
Joint Torque (Arm)	7	Nm	2
Joint Position (Hand)	1	tics	2
Joint Velocity (Hand)	1	tics/s	2
Force-Torque (Wrist)	6	N, Nm	2
Binary Grasp Sensor	1	au	2
TCP Pose	7	m, au	2
Camera images	$3 \times 64 \times 64 \times 3$	R/G/B value	0
Last Control Command	8	rad/s, tics/s	2

- **LIFT( $G$ ):**  $slin(G, 0.03, 0.10)$   
Increase z coordinate of an object more than 3cm relative to the table.
- **PLACE\_WIDE( $G, Y$ ):**  $stol(d(G, Y + [0, 0, 0.05]), 0.01, 0.20)$   
Bring green cube to a position 5cm above the yellow cube.
- **PLACE\_NARROW( $G, Y$ ):**  $stol(d(G, Y + [0, 0, 0.05]), 0.00, 0.01)$ :  
Like PLACE\_WIDE( $G, Y$ ) but more precise.
- **STACK( $G, Y$ ):**  $btol(d_{xy}(G, Y), 0.03) * btol(d_z(G, Y) + 0.05, 0.01) * (1 - GRASP)$   
Sparse binary reward for bringing the green cube on top of the yellow one (with 3cm tolerance horizontally and 1cm vertically) and disengaging the grasp sensor.
- **STACK\_AND\_LEAVE( $G, Y$ ):**  $stol(d_z(TCP, G) + 0.10, 0.03, 0.10) * STACK(G, Y)$   
Like STACK( $G, Y$ ), but needs to move the arm 10cm above the green cube.

**Ball-In-Cup** This task consists of a Sawyer robot arm mounted on a pedestal. A partially see-through cup structure with a radius of 11cm and height of 17cm is attached to the wrist flange. Between cup and wrist there is a ball bearing, to which a yellow ball of 4.9cm diameter is attached via a string of 46.5cm length (see Figure 4).

Most of the settings for the experiment align with the stacking task. The agent is provided with proprioception information for the arm (joint positions, velocities and torques), and the tool center point and cup positions computed via forward kinematics. It is also provided with two RGB camera images at  $64 \times 64$  resolution. At each timestep, a history

of two previous observations (except for the images) is provided to the agent, along with the last two joint control commands. The observation space is detailed in Table 8. All BIC experiments are run with 20 actors in parallel and reported over the current episodes generated by any actor. Episode lengths are up to 600 steps.

The position of the ball in the cup’s coordinate frame is available for reward computation, but not exposed to the agent. The robot arm is controlled in joint velocity mode at 20Hz. The action space for the agent is 4-dimensional, with only 4 out of 7 joints being actuated, in order to avoid self-collision. Details are provided in Table 5.

Table 7: Action space for the Sawyer Ball-in-Cup experiments.

Entry	Dims	Unit	Range
Rotational Joint Velocity for joints 1, 2, 6 and 7	4	rad/s	[-2, 2]

Table 8: Observations for the Sawyer Ball-in-Cup experiments. In the table,  $m$  denotes meters,  $rad$  denotes radians, and  $q$  refers to a quaternion in arbitrary units ( $au$ ). Note: the joint velocity and command represent the robot’s internal state; the 3 degrees of freedom that were fixed provide a constant input of 0.

Entry	Dims	Unit
Joint Position (Arm)	7	rad
Joint Velocity (Arm)	7	rad/s
TCP Pose	7	m, au
Camera images	$2 \times 64 \times 64 \times 3$	R/G/B value
Last Control Command	7	rad/s

Let  $B_A$  be the Cartesian position in meters of the ball in the cup’s coordinate frame (with an origin at the center of the cup’s bottom), along axes  $A \in \{x, y, z\}$ .

- **CATCH:**  $0.17 > B_z > 0$  and  $\|B_{xy}\|_2 < 0.11$   
Binary reward if the ball is inside the volume of the cup.
- **BALL\_ABOVE\_BASE:**  $B_z > 0$   
Binary reward if the ball is above the bottom plane of the cup.
- **BALL\_ABOVE\_RIM:**  $B_z > 0.17$   
Binary reward if the ball is above the top plane of the cup.
- **BALL\_NEAR\_MAX:**  $B_z > 0.3$   
Binary reward if the ball is near the maximum possible height above the cup.

- **BALL\_NEAR\_RIM**:  $1 - \tanh^2\left(\frac{\operatorname{atanh}(\sqrt{0.95})}{0.5}\right) \times \|B_{xyz} - (0, 0, 0.17)\|_2$   
Shaped distance of the ball to the center of the cup opening (0.95 loss at a distance of 0.5).

### B.3. Pre-training and Sequential Transfer Experiments

The sequential transfer experiments are performed with the same settings as their multitask equivalents. However, they rely on a pre-training step in which we take all but the final task in each domain and train HO2 to pre-train options which we then transfer with a new high-level controller on the final task. Fine-tuning of the options is enabled as we find that it produces slightly better performance. Only data used for the final training step is reported but all both approaches were trained for the same amount of data during pretraining until convergence. The variant with limited switches limits to 4 switches over a sequence length of 16.

### B.4. Locomotion experiments

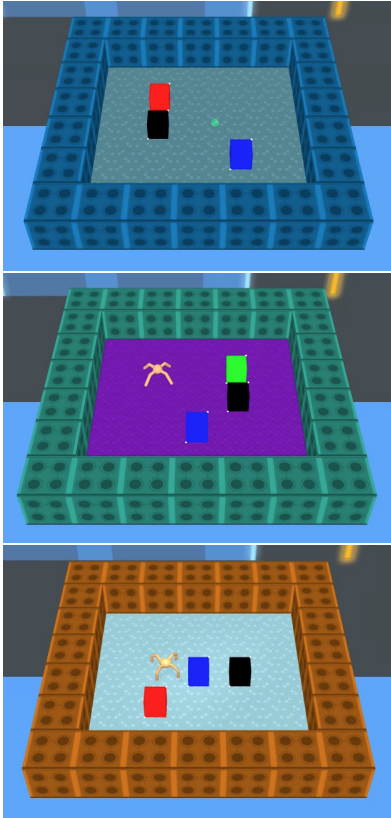


Figure 17: The environment used for simple locomotion tasks with Ball (top), Ant (center) and Quadruped (bottom).

Figure 17 shows examples of the environment for the different bodies used. In addition to proprioceptive agent state information (which includes the body height, position of the end-effectors, the positions and velocities of its joints

and sensor readings from an accelerometer, gyroscope and velocimeter attached to its torso), the state space also includes the ego-centric coordinates of all target locations and a categorical index specifying the task of interest. Table 9 contains an overview of the observations and action dimensions for this task. The agent receives a sparse reward of +60 if part of its body reaches a square surrounding the predicate location, and 0 otherwise. Both the agent spawn location and target locations are randomized at the start of each episode, ensuring that the agent must use both the task index and target locations to solve the task.

Table 9: Observations for the *go to one of 3 targets* task with Ball, Ant, and Quadruped.

Entry	Dimensionality
Task Index	3
Target locations	9
Proprioception (Ball)	16
Proprioception (Ant)	41
Proprioception (Quad)	57
Action Dim (Ball)	2
Action Dim (Ant)	8
Action Dim (Quad)	12

## C. Additional Derivations

In this section we explain the derivations for training option policies with options parameterized as Gaussian distributions. Each policy improvement step is split into two parts: non-parametric and parametric update.

### C.1. Non-parametric Option Policy Update

In order to obtain the non-parametric policy improvement we optimize the following equation:

$$\begin{aligned}
 & \max_q \mathbb{E}_{h_t \sim p(h_t)} [\mathbb{E}_{a_t, o_t \sim q} [Q_\phi(s_t, a_t, o_t)]] \\
 & s.t. \mathbb{E}_{h_t \sim p(h_t)} [\text{KL}(q(\cdot|h_t), \pi_\theta(\cdot|h_t))] < \epsilon_E \\
 & s.t. \mathbb{E}_{h_t \sim p(h_t)} [\mathbb{E}_{q(a_t, o_t|h_t)} [1]] = 1.
 \end{aligned}$$

for each step  $t$  of a trajectory, where  $h_t = \{s_t, a_{t-1}, s_{t-1}, \dots, a_0, s_0\}$  represents the history of states and actions and  $p(h_t)$  describes the distribution over histories for timestep  $t$ , which in practice are approximated via the use of a replay buffer  $\mathcal{D}$ . When sampling  $h_t$ , the state  $s_t$  is the first element of the history. The inequality constraint describes the maximum allowed KL divergence between intermediate update and previous parametric policy, while the equality constraint simply ensures that the intermediate update represents a normalized distribution.

Subsequently, in order to render the following derivations

more intuitive, we replace the expectations and explicitly use integrals. The Lagrangian  $L(q, \eta, \gamma)$  can now be formulated as

$$L(q, \eta, \gamma) = \iiint p(h_t)q(a_t, o_t|h_t)Q_\phi(s_t, a_t, o_t) \quad (13)$$

$$+ \eta \left( \epsilon_E - \iiint p(h_t)q(a_t, o_t|h_t) \log \frac{q(a_t, o_t|h_t)}{\pi_\theta(a_t, o_t|h_t)} \right)$$

$$+ \gamma \left( 1 - \iiint p(h_t)q(a_t, o_t|h_t) \log \pi_\theta(a_t, o_t|h_t) \right).$$

Next to maximize the Lagrangian with respect to the primal variable  $q$ , we determine its derivative as,

$$\frac{\partial L(q, \eta, \gamma)}{\partial q} = Q_\phi(a_t, o_t, s_t) - \eta \log q(a_t, o_t|h_t)$$

$$+ \eta \log \pi_\theta(a_t, o_t|h_t) - \eta - \gamma.$$

In the next step, we can set the left hand side to zero and rearrange terms to obtain

$$q(a_t, o_t|h_t) = \pi_\theta(a_t, o_t|h_t) \exp \left( \frac{Q_\phi(s_t, a_t, o_t)}{\eta} \right)$$

$$\exp \left( -\frac{\eta + \gamma}{\eta} \right).$$

The last exponential term represents a normalization constant for  $q$ , which we can formulate as

$$\frac{\eta + \gamma}{\eta} = \log \left( \iint \pi_\theta(a_t, o_t|h_t) \exp \left( \frac{Q_\phi(s_t, a_t, o_t)}{\eta} \right) \mathrm{d}o_t \mathrm{d}a_t \right). \quad (14)$$

In order to obtain the dual function  $g(\eta)$ , we insert the solution for the primal variable into the Lagrangian in Equation 13 which yields

$$L(q, \eta, \gamma) = \iiint p(h_t)q(a_t, o_t|h_t)Q_\phi(s_t, a_t, o_t) \quad (15)$$

$$+ \eta \left( \epsilon_E - \iiint p(h_t)q(a_t, o_t|h_t) \log \frac{\pi_\theta(a_t, o_t|h_t) \exp \left( \frac{Q_\phi(s_t, a_t, o_t)}{\eta} \right) \exp \left( -\frac{\eta + \gamma}{\eta} \right)}{\pi_\theta(a_t, o_t|h_t)} \right)$$

$$+ \gamma \left( 1 - \iiint p(h_t)q(a_t, o_t|h_t) \log \pi_\theta(a_t, o_t|h_t) \right).$$

We expand the equation and rearrange to obtain

$$L(q, \eta, \gamma) = \iiint p(h_t)q(a_t, o_t|h_t)Q_\phi(s_t, a_t, o_t) \quad (16)$$

$$- \eta \iiint p(h_t)q(a_t, o_t|h_t) \left[ \frac{Q_\phi(s_t, a_t, o_t)}{\eta} + \log \pi_\theta(a_t, o_t|h_t) - \frac{\eta + \gamma}{\eta} \right] \mathrm{d}o_t \mathrm{d}a_t \mathrm{d}h_t$$

$$+ \eta \epsilon_E + \eta \iiint p(h_t)q(a_t, o_t|h_t) \log \pi_\theta(a_t, o_t|h_t) \mathrm{d}o_t \mathrm{d}a_t \mathrm{d}h_t$$

$$+ \gamma \left( 1 - \iiint p(h_t)q(a_t, o_t|h_t) \mathrm{d}o_t \mathrm{d}a_t \mathrm{d}h_t \right).$$

In the next step, most of the terms cancel out and after additional rearranging of the terms we obtain

$$L(q, \eta, \gamma) = \eta \epsilon_E + \eta \int p(h_t) \frac{\eta + \gamma}{\eta} \mathrm{d}h_t.$$

We have already calculated the term inside the integral in Equation 14, which we now insert to obtain

$$g(\eta) = \min_q L(q, \eta, \gamma) \quad (15)$$

$$= \eta \epsilon_E + \eta \int p(h_t) \log \left( \iint \pi_\theta(a_t, o_t|h_t) \exp \left( \frac{Q_\phi(s_t, a_t, o_t)}{\eta} \right) \mathrm{d}o_t \mathrm{d}a_t \right) \mathrm{d}h_t$$

$$= \eta \epsilon_E + \eta \mathbb{E}_{h_t \sim p(h_t)} \left[ \log \left( \mathbb{E}_{a_t, o_t \sim \pi_\theta} \left[ \exp \left( \frac{Q_\phi(s_t, a_t, o_t)}{\eta} \right) \right] \right) \right].$$

The dual in Equation 15 can finally be minimized with respect to  $\eta$  based on samples from the replay buffer and policy.

## C.2. Parametric Option Policy Update

After obtaining the non-parametric policy improvement, we can align the parametric option policy to the current non-parametric policy. As the non-parametric policy is represented by a set of samples from the parametric policy with additional weighting, this step effectively employs a type of critic-weighted maximum likelihood estimation. In addition, we introduce regularization based on a distance function  $\mathcal{T}$  which has a trust-region effect for the update and stabilizes learning.



$$\begin{aligned}
 \theta_{new} &= \arg \min_{\theta} \mathbb{E}_{h_t \sim p(h_t)} \left[ \text{KL}(q(a_t, o_t | h_t) \| \pi_{\theta}(a_t, o_t | h_t)) \right] \\
 &= \arg \min_{\theta} \mathbb{E}_{h_t \sim p(h_t)} \left[ \mathbb{E}_{a_t, o_t \sim q} \left[ \log q(a_t, o_t | h_t) \right. \right. \\
 &\quad \left. \left. - \log \pi_{\theta}(a_t, o_t | h_t) \right] \right] \\
 &= \arg \max_{\theta} \mathbb{E}_{h_t \sim p(h_t), a_t, o_t \sim q} \left[ \log \pi_{\theta}(a_t, o_t | h_t) \right], \\
 &\text{s.t. } \mathbb{E}_{h_t \sim p(h_t)} \left[ \mathcal{T}(\pi_{\theta_{new}}(\cdot | h_t) | \pi_{\theta}(\cdot | h_t)) \right] < \epsilon_M,
 \end{aligned}$$

where  $h_t \sim p(h_t)$  is a trajectory segment, which in practice sampled from the dataset  $\mathcal{D}$ ,  $\mathcal{T}$  is an arbitrary distance function between the new policy and the previous policy.  $\epsilon_M$  denotes the allowed change for the policy. We again employ Lagrangian Relaxation to enable gradient based optimization of the objective, yielding the following primal:

$$\begin{aligned}
 \max_{\theta} \min_{\alpha > 0} L(\theta, \alpha) &= \mathbb{E}_{h_t \sim p(h_t), a_t, o_t \sim q} \left[ \log \pi_{\theta}(a_t, o_t | h_t) \right] \\
 &\quad + \alpha \left( \epsilon_M - \mathbb{E}_{h_t \sim p(h_t)} \left[ \mathcal{T}(\pi_{\theta_{new}}(\cdot | h_t), \pi_{\theta}(\cdot | h_t)) \right] \right).
 \end{aligned} \tag{16}$$

We can solve for  $\theta$  by iterating the inner and outer optimization programs independently. In practice we find that it is most efficient to update both in parallel.

We also define the following distance function between old and new option policies

$$\mathcal{T}(\pi_{\theta_{new}}(\cdot | h_t), \pi_{\theta}(\cdot | h_t)) = \mathcal{T}_H(h_t) + \mathcal{T}_T(h_t) + \mathcal{T}_L(h_t)$$

$$\begin{aligned}
 \mathcal{T}_H(h_t) &= \text{KL}(\text{Cat}(\{\alpha_{\theta_{new}}^j(h_t)\}_{j=1 \dots M}) \| \\
 &\quad \text{Cat}(\{\alpha_{\theta}^j(h_t)\}_{j=1 \dots M})) \\
 \mathcal{T}_T(h_t) &= \frac{1}{M} \sum_{j=1}^M \text{KL}(\text{Cat}(\{\beta_{\theta_{new}}^{ij}(h_t)\}_{j=1 \dots 2}) \| \\
 &\quad \text{Cat}(\{\beta_{\theta}^{ij}(h_t)\}_{j=1 \dots 2})) \\
 \mathcal{T}_L(h_t) &= \frac{1}{M} \sum_{j=1}^M \text{KL}(\mathcal{N}(\mu_{\theta_{new}}^j(h_t), \Sigma_{\theta_{new}}^j(h_t)) \| \\
 &\quad \mathcal{N}(\mu_{\theta}^j(h_t), \Sigma_{\theta}^j(h_t)))
 \end{aligned}$$

where  $\mathcal{T}_H$  evaluates the KL between the categorical distributions of the high-level controller,  $\mathcal{T}_T$  is the average KL between the categorical distributions of the all termination conditions, and  $\mathcal{T}_L$  corresponds to the average KL across Gaussian components. In practice, we can exert additional control over the convergence of model components by applying different  $\epsilon_M$  to different model parts (high-level controller, termination conditions, options).

### C.3. Transition Probabilities for Option and Switch Indices

The transitions for option  $o$  and switch index  $n$  are given by:

$$\begin{aligned}
 p(o_t, n_t | s_t, o_{t-1}, n_{t-1}) &= \\
 \begin{cases} (1 - \beta(s_t, o_{t-1})) & \text{if } n_t = n_{t-1}, o_t = o_{t-1} \\ \beta(s_t, o_{t-1}) \pi^C(o_t | s_t) & \text{if } n_t = n_{t-1} + 1 \\ 0 & \text{otherwise} \end{cases} \tag{17}
 \end{aligned}$$